

Segregation of receptor–ligand complexes in cell adhesion zones: phase diagrams and the role of thermal membrane roughness

B Różycki^{1,2,3}, R Lipowsky¹ and T R Weikl^{1,3}

¹ Department of Theory and Bio-Systems, Max Planck Institute of Colloids and Interfaces, 14424 Potsdam, Germany

² Laboratory of Chemical Physics, National Institute of Diabetes and Digestive and Kidney Diseases, National Institutes of Health, Bethesda, MD 20892-0520, USA

E-mail: bartosz.rozycki@mpikg.mpg.de and thomas.weikl@mpikg.mpg.de

New Journal of Physics **12** (2010) 095003 (22pp)

Received 8 May 2010

Published 8 September 2010

Online at <http://www.njp.org/>

doi:10.1088/1367-2630/12/9/095003

Abstract. The adhesion zone of immune cells, the ‘immunological synapse’, exhibits characteristic domains of receptor–ligand complexes. The domain formation is probably caused by a length difference of the receptor–ligand complexes, and has been investigated in experiments in which T cells adhere to supported membranes with anchored ligands. For supported membranes with two types of anchored ligands, MHCp and ICAM1, which bind to the T-cell receptor (TCR) and the receptor LFA1 in the cell membrane, the coexistence of domains of the TCR–MHCp and LFA1–ICAM1 complexes in the cell adhesion zone has been observed for a wide range of ligand concentrations and affinities. For supported membranes with long and short ligands that bind to the same cell receptor CD2, in contrast, domain coexistence has been observed for a quite narrow ratio of ligand concentrations. In this paper, we determine detailed phase diagrams for cells adhering to supported membranes with a statistical–physical model of cell adhesion. We find a characteristic difference between the adhesion scenarios in which two types of ligands in a supported membrane bind (i) to the same cell receptor or (ii) to two different cell receptors, which helps us to explain the experimental observations. Our phase diagrams fully include thermal shape fluctuations of the cell membranes on nanometer scales, which lead to a critical point for the domain formation and to a cooperative binding of the receptors and ligands.

³ Authors to whom any correspondence should be addressed.

Contents

1. Introduction	2
2. Statistical–physical description of cell adhesion	3
3. Adhesion via a single type of receptor–ligand complexes	5
3.1. Interaction energy of receptors and ligands	5
3.2. Effective adhesion potential	6
3.3. Area fraction P_b of the membranes within the binding range of receptors and ligands	7
3.4. Concentrations of bound and unbound receptors of an adhering cell	8
4. Two types of membrane-anchored ligands adhering to the same cell receptor	8
4.1. Interaction energy of receptors and ligands	8
4.2. Effective adhesion potential	10
4.3. Phase diagram	10
5. Two types of membrane-anchored ligands adhering to different cell receptors	12
5.1. Interaction energy of receptors and ligands and effective adhesion potential	12
5.2. Phase diagram	14
6. Discussion and conclusions	17
References	19

1. Introduction

Cell adhesion is mediated by the specific binding of a variety of membrane-anchored receptor and ligand molecules. In 1990, Springer suggested that the length difference of receptor–ligand complexes in the contact zone of immune cells may lead to segregation, i.e. to the formation of domains within the cell contact zone that contain receptor–ligand complexes with different lengths [1]. The ‘length’ of a receptor complex here is the intermembrane distance or local membrane separation at the site of the complex. A length difference between receptor–ligand complexes leads to an indirect, membrane-mediated repulsion of the complexes because the membranes have to bend to compensate for the mismatch, which costs bending energy. Important receptor–ligand complexes in T-cell adhesion are the TCR–MHCp complex with a length of about 13 nm [2], the CD2–CD48 complex with the same length of 13 nm [3]–[5] and the LFA1–ICAM1 complex with a length of about 40 nm [6]. In 1998 and 1999, the contact zone of T cells was indeed found to contain domains that contain either the short TCR–MHCp or the long LFA1–ICAM1 complexes [7, 8]. As expected from their length, the CD2–CD48 complexes are located within the TCR–MHCp domains [5]. However, the question of whether the domain formation is predominantly caused by the length mismatch of receptor–ligand complexes is complicated by the role of the actin cytoskeleton, which polarizes during T-cell adhesion and transports clusters of TCR–MHCp complexes towards the center of the cell contact zone [9]–[11], and by additional, direct protein–protein interactions [12]. The domain formation is closely linked to T-cell activation, with TRC clusters forming within seconds of T-cell adhesion triggering the first activation signals [9, 13].

Direct evidence for a central role of the length of receptor–ligand complexes comes from experiments in which these lengths are altered by protein engineering [5, 14]. Milstein *et al* [5] have considered variants of the protein CD48 with four and five immunoglobulin-like (Ig-like)

domains. The CD48 variants are longer than the CD48 wildtype, which contains only two Ig-like domains. The CD48 wildtype and both CD48 variants bind to CD2 on T cells. From electron micrographs of the contact zone between T cells and supported membranes that contain one of the three CD48 types, Milstein *et al* found that the length of the CD2–CD48 complex is 12.8 ± 1.4 nm for wildtype CD48, 14.2 ± 1.2 nm for the CD48 variant with four Ig-like domains and 15.6 ± 1.4 nm for the variant with five Ig-like domains. In fluorescence experiments of T cells on supported membranes that contain mixtures of two of the three CD48 types, Milstein *et al* observed that CD2–CD48 wildtype complexes segregate from both CD2–CD48 variant complexes. The segregation seems to be driven by the length difference of the complexes since the T-cell cytoskeleton can only ‘act on’ CD2 and can thus hardly ‘discriminate’ between the different complexes. However, Milstein *et al* observe domain coexistence in the contact zone only within a narrow range of concentration ratios of CD48 wildtype and CD48 variants. For T cells adhering to supported membranes with MHCp and ICAM1, in contrast, domain coexistence has been observed for quite a wide range of MHCp and ICAM1 concentrations and affinities [8, 9, 15].

In this paper, we calculate detailed phase diagrams for cells adhering to supported membranes with anchored ligands. We consider two general adhesion scenarios. In the first scenario, long and short ligands in the supported membrane bind to the same cell receptor (see section 4), as in the experiments of Milstein *et al* [5], in which CD48 wildtype and a CD48 variant in the supported membrane both bind to CD2 in the T-cell membrane. In the second scenario, two types of ligands in the supported membrane bind to two types of receptors in the cell membrane (see section 5), as in experiments in which MHCp and ICAM1 in the supported membrane bind to T-cell receptor (TCR) and LFA1 in the T-cell membrane. We find a characteristic difference between the phase diagrams in the two scenarios (see figure 5). In the first scenario, domain coexistence only occurs along a coexistence line. In the second scenario, in contrast, domain coexistence occurs in a wide coexistence region. Our phase diagrams thus help us to understand why Milstein *et al* observe domain coexistence only within a narrow range of concentration ratios.

Our calculations are based on a statistical–physical model of cell adhesion (see section 2). In this model, the membranes are described as elastic sheets discretized into small patches that can contain single receptor or ligand molecules [16]–[19]. The binding and domain formation of receptor–ligand complexes is affected by thermally excited shape fluctuations of the membranes on the nanometer scale. These shape fluctuations lead to a critical point for the segregation of long and short receptor–ligand complexes [19, 20]. The critical point depends on the length difference of the complexes, on the concentrations and affinities of the receptors and ligands and on the bending rigidity of the membranes (see section 4). The critical point constitutes a threshold for segregation, or domain formation, and may help us to understand why Milstein *et al* have observed segregation of wildtype CD48 from each of the two CD48 variants, but not segregation of the two CD48 variants [5]. In addition, the membrane shape fluctuations on the nanoscale lead to a cooperative binding of receptor–ligand complexes [21] (see section 3).

2. Statistical–physical description of cell adhesion

Cell adhesion involves length scales that differ by orders of magnitude (see figure 1). The diameters of the cell and cell contact zone have values of several micrometers, while the average separation of the membranes within the contact zone is typically tens of nanometers.

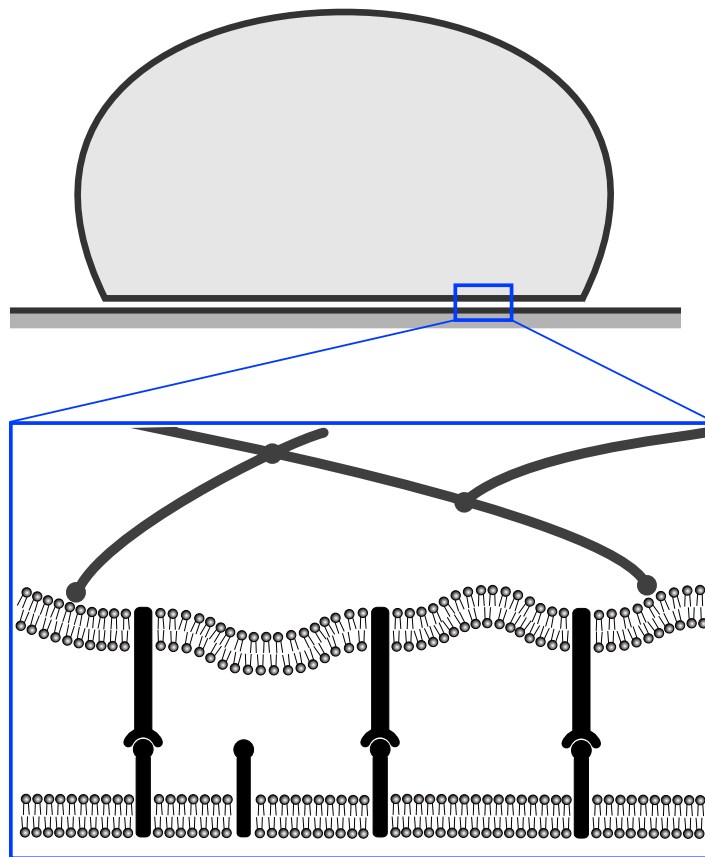


Figure 1. A cell adhering to a supported membrane with anchored ligands that bind to receptors in the cell membrane. The binding of receptors and ligands in the cell adhesion zone is affected by membrane shape deformations and fluctuations on nanometer scales, which are dominated by the bending rigidity of the cell membrane. The immune cell receptors are typically mobile along the membrane and not or only weakly [11] coupled to the cytoskeleton.

Other important length scales in the cell contact zone are the average distance between receptor–ligand bonds, and the binding width of receptor and ligand molecules. The binding width is the difference between the smallest and the largest local membrane separation at which the molecules can bind. The binding width of the typically quite stiff receptor and ligand proteins that mediate cell adhesion is much smaller than the length of the proteins.

The binding equilibrium and segregation of receptor–ligand complexes in cell contact zones is affected by membrane shape deformations and fluctuations. Since bound receptor–ligand complexes constrain the local separation of the membranes, the relevant deformations and fluctuations of the membranes occur on lateral length scales smaller than the average distance between neighboring pairs of complexes, which is about 100 nm for complex concentrations of about 100 per square micrometer [8]. It is reasonable to assume that the elasticity of the membranes is dominated by their bending rigidity on these length scales. The binding rigidity κ dominates over the membrane tension σ on lateral length scales smaller than the crossover length $\sqrt{\kappa/\sigma}$ [22], which is of the order of several 100 nm for cell membranes [23]. The cytoskeletal elasticity [24]–[27] contributes on length scales larger than the average distance

between the cytoskeletal anchors in the membrane, which may be about 100 nm [28]. The bending rigidity thus is likely to dominate over the lateral tension and the cytoskeletal elasticity on lateral length scales up to 100 nm relevant here.

We have developed discrete models for the adhesion of membranes via anchored receptors and ligands [16, 18, 19, 29]. In discrete models, the two apposing membranes in the contact zone of cells or vesicles are divided into small patches [16]–[18], [20, 23], [29]–[36]. In our models, the rigidity-dominated elasticity of the membranes in the contact zones of cells or vesicles is described by the equation [16, 18]

$$\mathcal{H}_{\text{el}}\{l\} = \frac{\kappa}{2a^2} \sum_i (\Delta_d l_i)^2, \quad (1)$$

where l_i is the local separation of the apposing membrane patches i . The elastic energy depends on the mean curvature $(\Delta_d l_i)/(2a^2)$ of the separation field l_i with the discretized Laplacian $\Delta_d l_i = l_{i1} + l_{i2} + l_{i3} + l_{i4} - 4l_i$. Here, l_{i1} to l_{i4} are the membrane separations at the four nearest-neighbor patches of membrane patch i on the quadratic array of patches. The linear size a of the membrane patches is chosen to be about 5 nm to capture the whole spectrum of bending deformations of the lipid membranes [37]. The ‘effective bending rigidity’ of the two membranes with rigidities κ_1 and κ_2 is $\kappa = \kappa_1 \kappa_2 / (\kappa_1 + \kappa_2)$. If one of the membranes, e.g. membrane 2, is a planar supported membrane, the effective bending rigidity κ equals the rigidity κ_1 of the apposing membrane since the rigidity κ_2 of the supported membrane is taken to be much larger than κ_1 .

The overall energy of the membranes in the cell contact zone

$$\mathcal{H}\{l, n, m\} = \mathcal{H}_{\text{el}}\{l\} + \mathcal{H}_{\text{int}}\{l, n, m\} \quad (2)$$

is the sum of the elastic energy $\mathcal{H}_{\text{el}}\{l\}$ and interaction energy $\mathcal{H}_{\text{int}}\{l, n, m\}$. The interaction energy depends on the distribution n of the receptors in membrane 1, on the distribution m of the receptors in membrane 2 and on the separation field l of the membranes. In our models, each patch of the discrete membranes can only be occupied by one receptor or ligand molecule. Mobile receptor and ligand molecules diffuse by ‘hopping’ from patch to patch, and the thermal fluctuations of the membranes are reflected in variations of the local separation of apposing membrane patches. A receptor can bind to a ligand molecule if the ligand is located in the membrane patch apposing the receptor and if the local separation of the membranes is close to the length of the receptor–ligand complex (see figure 2 and below). In discrete models, the receptor and ligand molecules are taken into account as individual molecules. In continuum models, in contrast, the distributions of receptor and ligand molecules on the membranes are described by continuous concentration profiles [38]–[48].

3. Adhesion via a single type of receptor–ligand complexes

3.1. Interaction energy of receptors and ligands

We first consider the case in which the adhesion is mediated by a single type of receptor–ligand complexes. Examples of this case are (i) cells adhering to supported membranes that contain a single type of ligand [5], [49]–[51] and (ii) vesicles with anchored receptors that adhere to supported membranes or surfaces with complementary ligands [35], [52]–[62]. The interactions of receptors and ligands within the contact zone of the cell or vesicle are described by the

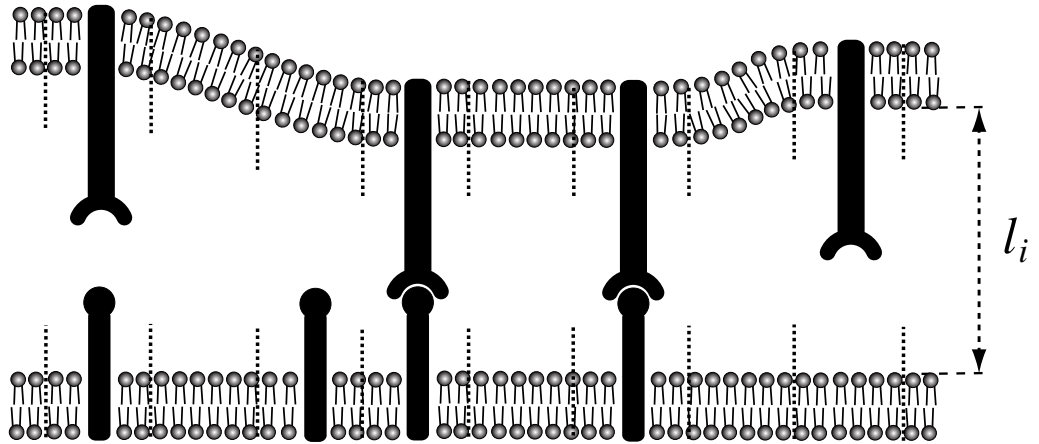


Figure 2. A supported membrane with anchored ligands (bottom) that bind to receptors in an apposing cell or vesicle membrane (top). In our model, the membranes are discretized in small patches, which can contain single receptor or ligand molecules. The shape and thermal fluctuations of the cell or vesicle membrane in the adhesion zone are described by the local separations l_i of apposing membrane patches i . A receptor can bind to a ligand molecule (i) if the ligand is located in the membrane patch apposing the receptor and (ii) if the local membrane separation l_i is close to the length of the receptor–ligand complex.

interaction energy [17, 21]

$$\mathcal{H}_{\text{int}}\{l, n, m\} = \sum_i n_i m_i V(l_i) \quad (3)$$

in our model. Here, the occupation number $n_i = 1$ or 0 indicates whether a receptor is present or absent in membrane patch i of the cell, and $m_i = 1$ or 0 indicates whether a ligand is present or absent in patch i of the apposing membrane. Receptor and ligand molecules in apposing patches i of the membranes interact with the potential $V(l_i)$. For simplicity, we describe this interaction by the square-well potential

$$\begin{aligned} V(l_i) &= -U \quad \text{for } l_0 - l_{\text{we}}/2 < l_i < l_0 + l_{\text{we}}/2 \\ &= 0 \quad \text{otherwise,} \end{aligned} \quad (4)$$

which depends on the binding energy $U > 0$ and the length l_0 and binding width l_{we} of a receptor–ligand complex. A receptor thus binds to an apposing ligand with energy $-U$ if the local separation l_i of the membranes is within the binding range $l_0 \pm l_{\text{we}}/2$.

3.2. Effective adhesion potential

The binding equilibrium of the membranes in the contact zone can be determined from the free energy $\mathcal{F} = -k_B T \ln \mathcal{Z}$, where \mathcal{Z} is the partition function of the system, k_B is Boltzmann's constant and T is the temperature. The partition function \mathcal{Z} is the sum over all possible membrane configurations, with each configuration $\{l, n, m\}$ weighted by the Boltzmann factor $\exp[-\mathcal{H}\{l, n, m\}/k_B T]$. A membrane configuration in the contact zone is specified by the

separation field l of the membranes, the distribution m of the receptors in the cell membrane and the distribution n of ligands in the apposing membrane. In our model, the partial summation in the partition function \mathcal{Z} over all possible distributions m and n of receptors and ligands can be performed exactly, which leads to an effective adhesion potential. The effective adhesion potential $V_{\text{ef}}(l_i)$ is a square-well potential with (i) the same binding range l_{we} as the receptor–ligand interaction (5) and (ii) an effective potential depth U_{ef} that depends on the concentrations and binding energy U of receptors and ligands [17, 18, 21]:

$$\begin{aligned} V_{\text{ef}}(l_i) &= -U_{\text{ef}} \quad \text{for } l_0 - l_{\text{we}}/2 < l_i < l_0 + l_{\text{we}}/2 \\ &= 0 \quad \text{otherwise.} \end{aligned} \quad (5)$$

For typical concentrations of receptors and ligands in cell adhesion zones up to 100 or several hundreds of molecules per square micrometer, the average distance between neighboring pairs of receptor and ligand molecules is much smaller than the width of the molecules. For these small concentrations, the effective binding energy of the membranes is [21]

$$U_{\text{ef}} \approx k_{\text{B}}T a^2 e^{U/k_{\text{B}}T} [R][L], \quad (6)$$

where $[R]$ is the area concentration of unbound receptors in the cell membrane, and $[L]$ is the area concentration of unbound ligands in the apposing membrane. The binding equilibrium in the contact zone thus can be determined from considering two membranes with the elastic energy (1) that interact via an effective adhesion potential with well depth U_{ef} and width l_{we} .

3.3. Area fraction P_{b} of the membranes within the binding range of receptors and ligands

Receptor–ligand complexes can only form at membrane patches with a local separation within the binding range $l_0 \pm l_{\text{we}}/2$ of the receptors and ligands (see equation (5)). The area concentration $[RL]$ of the receptor–ligand complexes in the contact zone is therefore proportional to the fraction P_{b} of these membrane patches [21]:

$$[RL] \approx P_{\text{b}} K [R][L]. \quad (7)$$

Here, K is the equilibrium constant for receptor–ligand binding within this membrane fraction. In our model, the equilibrium constant is $K = a^2 e^{U/k_{\text{B}}T}$.

In equilibrium, the fraction P_{b} of membrane patches with a local separation within receptor–ligand binding range depends on the effective binding energy U_{ef} , the binding width l_{we} , the effective rigidity κ of the membranes and the temperature T . We have found that the effect of these four quantities on P_{b} can be captured by a single dimensionless quantity, the rescaled effective potential depth [21]

$$u \equiv U_{\text{ef}} \kappa l_{\text{we}}^2 / (k_{\text{B}}T)^2 \approx (\kappa / k_{\text{B}}T) l_{\text{we}}^2 K [R][L]. \quad (8)$$

To a first approximation, the membrane fraction P_{b} depends only on u for typical lengths and concentrations of receptor–ligand complexes in cell adhesion zones. In cell adhesion zones, direct contacts between the membranes can be neglected since the average separation of the membranes, which depends on the length l_0 of the complexes, is typically larger than the thermal membrane roughness [21].

From Monte Carlo simulations, we have found that the functional dependence of the area fraction P_{b} on the rescaled potential depth u is well described by

$$P_{\text{b}} \approx \frac{u}{c_1 + u} \quad (9)$$

with the dimensionless coefficient $c_1 \simeq 0.071$ [21]. The membrane fraction P_b increases with u and thus increases with the effective binding energy U_{ef} and the effective bending rigidity κ . The reason for this increase is that the roughness of the membranes resulting from thermal shape fluctuations decreases with U_{ef} and κ . The membrane fraction P_b decreases with the temperature T since the roughness increases with T . The thermal roughness, defined as the standard deviation of the local membrane separation from its average, is the characteristic length scale for membrane excursions in the perpendicular direction. The membrane fraction P_b within receptor–ligand binding range is much smaller than 1 if the roughness is large compared to the binding width l_{we} of the complexes and close to 1 if the roughness is small compared to l_{we} .

3.4. Concentrations of bound and unbound receptors of an adhering cell

From equations (7)–(9), we obtain the relation [21]

$$[RL] \approx \frac{\kappa l_{\text{we}}^2 K^2 [R]^2 [L]^2}{c_1 k_B T + \kappa l_{\text{we}}^2 K [R][L]} \quad (10)$$

between the area concentration $[RL]$ of bound receptor–ligand complexes in the contact zone and the area concentrations $[R]$ and $[L]$ of unbound receptors and ligands. This nonlinear relation reflects the cooperative binding of receptors and ligands. This cooperativity arises because the binding of receptors and ligands suppresses thermal membrane fluctuations and, thus, smoothes the membranes, which facilitates the binding of additional receptors and ligands (see figure 3).

The total number N of receptors in the cell membrane is constant. The concentrations of bound and unbound receptors are therefore connected by the additional relation [19]

$$N \approx [R]A + [RL]A_c, \quad (11)$$

where A is the total area of the cell membrane and A_c the contact area. We have neglected here the area occupied by bound receptor–ligand complexes since this area is small compared to the total contact area A_c for typical concentrations in cell adhesion zones. The concentrations of unbound receptors within and outside of the contact area are then equal. Together, the two relations (10) and (11) determine the concentration $[R]$ of unbound receptors and the concentration $[RL]$ of bound receptors in the contact zone.

4. Two types of membrane-anchored ligands adhering to the same cell receptor

4.1. Interaction energy of receptors and ligands

In recent experiments by Milstein *et al* [5], long and short ligands anchored to a supported membrane bind to the same receptor of an adhering T cell. These ligands are wildtype CD48 and elongated CD48 variants, and the receptor in the T cell membrane is CD2. In our model, this situation is described by the interaction energy

$$\mathcal{H}_{\text{int}}\{l, n, m\} = \sum_i n_i (\delta_{m_i,1} V_1(l_i) + \delta_{m_i,2} V_2(l_i)) \quad (12)$$

for the two apposing membranes in the cell contact zone. Here, the occupation number $m_i = 1, 2$ or 0 indicates whether a ligand L_1 of type 1, a ligand L_2 of type 2 or no ligand is present in patch i of the supported membrane and $n_i = 1$ or 0 indicates whether a receptor R is present or

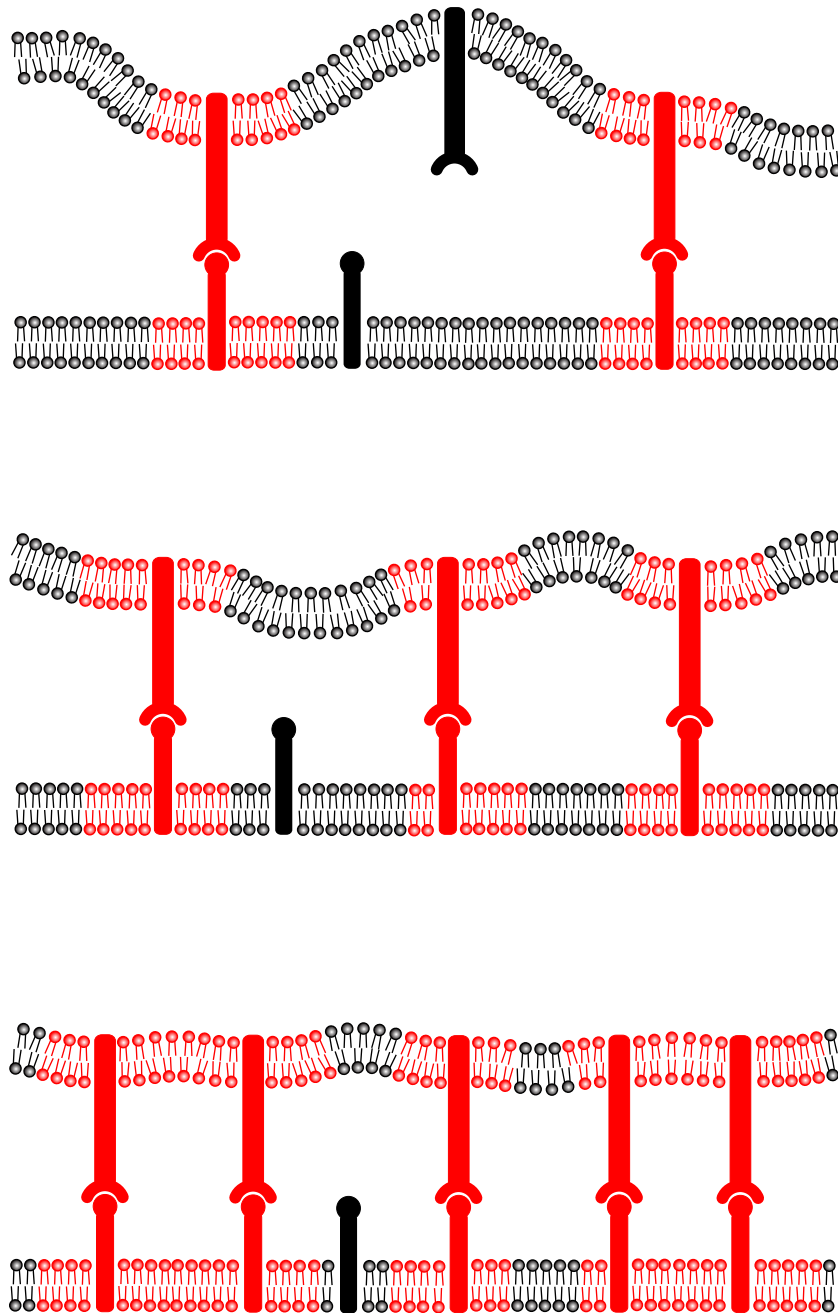


Figure 3. An important quantity is the area fraction P_b of the membranes within binding separation of the receptors and ligands. The area fraction P_b (shown in red) increases with the concentrations of receptors and ligands, since the formation of receptor–ligand bonds ‘smooths out’ thermal membrane shape fluctuations. The ‘smoothing’ facilitates the formation of additional receptor–ligand bonds and, thus, leads to a binding cooperativity [21].

not in the apposing patch i of the cell membrane. The Kronecker symbol $\delta_{i,j}$ equals 1 for $i = j$ and is equal to 0 for $i \neq j$. The potential V_1 thus describes the interaction of the receptor R with the ligand protein L_1 , and the potential V_2 the interaction between R and L_2 . For simplicity, V_1

and V_2 are again taken to be

$$\begin{aligned} V_1(l_i) &= U_1 \quad \text{for } l_1 - l_{\text{we}}/2 < l_i < l_1 + l_{\text{we}}/2 \\ &= 0 \quad \text{otherwise} \end{aligned} \quad (13)$$

and

$$\begin{aligned} V_2(l_i) &= U_2 \quad \text{for } l_2 - l_{\text{we}}/2 < l_i < l_2 + l_{\text{we}}/2 \\ &= 0 \quad \text{otherwise,} \end{aligned} \quad (14)$$

with binding energies U_1 and U_2 and equilibrium lengths $l_1 < l_2$ of the complexes RL_1 and RL_2 . We have assumed here that the two complexes have the same binding width l_{we} .

4.2. Effective adhesion potential

As in section 3.2, the summations over all possible distributions m and n of receptors and ligands in the partition function of the model lead to an effective adhesion potential [19, 20]. The effective adhesion potential now is a double-well potential (see figure 4). Both wells have the same width l_{we} as the potentials (13) and (14). The well with its center at the membrane separation $l_i = l_1$ reflects the interactions of the receptors R with the shorter ligands L_1 , and the well centered at $l_i = l_2$ reflects the interactions of the receptors and the longer ligands L_2 . In analogy to equation (6), the depths of the two wells

$$U_1^{\text{ef}} \approx k_{\text{B}}T K_1 [R][L_1] \quad (15)$$

and

$$U_2^{\text{ef}} \approx k_{\text{B}}T K_2 [R][L_2] \quad (16)$$

depend on the concentrations $[R]$, $[L_1]$ and $[L_2]$ of unbound receptors and ligands and on the binding constants $K_1 = a^2 e^{U_1/k_{\text{B}}T}$ and $K_2 = a^2 e^{U_2/k_{\text{B}}T}$ for receptors and ligands within the appropriate binding ranges [19, 20]. The binding equilibrium of the receptors R and ligands L_1 and L_2 in the contact zone can thus be determined by considering two apposing membranes with elastic energy (1) that interact via an effective double-well potential with well depths U_1^{ef} and U_2^{ef} given by equations (15) and (16).

4.3. Phase diagram

If the two wells of the effective adhesion potential are relatively shallow, thermal membrane fluctuations can easily drive membrane segments to cross from one well to the other. If the two wells are deep, the crossing of membrane segments from one well to the other well is hindered by the potential barrier of width l_{ba} between the wells (see figure 4). The potential barrier induces a line tension between adjacent membrane segments that are bound in different wells [63]. Beyond a critical depth of the potential wells, the line tension leads to the formation of large membrane domains that are bound in well 1 or well 2. Within each domain, the adhesion of the membranes is predominantly mediated either by the receptor–ligand complexes RL_1 or by the complexes RL_2 .

We have previously found that the critical potential depth for domain formation is

$$U_c^{\text{ef}} \approx \frac{c(k_{\text{B}}T)^2}{\kappa l_{\text{we}} l_{\text{ba}}}, \quad (17)$$

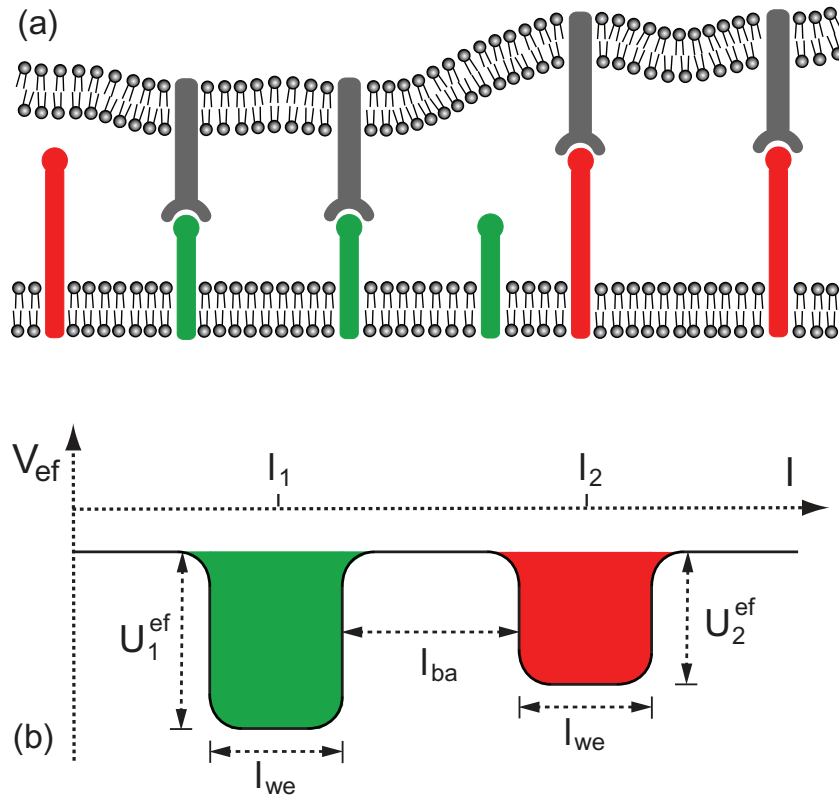


Figure 4. (a) A supported membrane with short (green) ligands L_1 and long (red) ligands L_2 that bind to the same receptor R in the cell membrane (top). (b) The interactions of the receptors and ligands lead to an effective double-well adhesion potential V_{ef} of the membranes. The potential well 1 at small membrane separations l reflects the interactions of the receptors with the short ligands, and the potential well 2 at larger membrane separations the interactions with the long ligands. The depths U_1^{ef} and U_2^{ef} of the two potential wells depend on the concentrations and binding constants of the receptors and ligands (see equations (15) and (16)). The wells have the same width l_{we} as the receptor–ligand interactions (13) and (14), and a separation $l_{\text{ba}} = l_2 - l_1 - l_{\text{we}}$ that depends on the difference between the equilibrium lengths l_1 and l_2 of the complexes RL_1 and RL_2 .

with the prefactor $c = 0.225 \pm 0.02$ determined by Monte Carlo simulations [20]. Domain formation in the contact zone or, in other words, segregation of the complexes RL_1 and RL_2 can only occur if the effective potential depths U_1^{ef} and U_2^{ef} exceed the critical potential depth U_c^{ef} . The critical potential depth depends on the temperature T and the bending rigidity κ , as well as on the width l_{we} and separation l_{ba} of the two potential wells. In deriving equation (17), we have neglected direct membrane–membrane contacts, which is reasonable for typical concentrations and lengths of receptor–ligand complexes in cell adhesion zones [20, 21]. For these complex concentrations and lengths, the thermal membrane roughness is smaller than the lengths of the receptor–ligand complexes.

Domain coexistence occurs for equal depths

$$U_1^{\text{ef}} = U_2^{\text{ef}} \quad (18)$$

of the potential wells if the two wells have the same width l_{we} as in figure 4. With equations (15) and (16), this coexistence condition implies that domain coexistence occurs along the line with

$$K_1[L_1] = K_2[L_2] \quad (19)$$

in the $[L_1]$ – $[L_2]$ -plane. The line has the slope K_1/K_2 and ends at a critical point (see the phase diagram in figure 5(a)). For $U_1^{\text{ef}} > U_2^{\text{ef}}$, we have $K_1[L_1] > K_2[L_2]$. The adhesion is then dominated by the short complexes RL_1 throughout the cell contact zone. For $U_1^{\text{ef}} < U_2^{\text{ef}}$, in contrast, the adhesion is dominated by the long complexes RL_2 in the whole contact zone. If the supported membrane is much larger than the cell contact zone, it seems reasonable to assume that the concentrations $[L_1]$ and $[L_2]$ of unbound ligands do not change upon adhesion since the ‘ligand reservoir’ in the supported membrane is large. The concentrations $[L_1]$ and $[L_2]$ in our model then correspond to the experimental ligand concentrations in the supported membrane prior to adhesion, and our phase diagram in figure 5(a) to the phase diagram in figure 7 of [5]; see the discussion section.

5. Two types of membrane-anchored ligands adhering to different cell receptors

5.1. Interaction energy of receptors and ligands and effective adhesion potential

Several experimental groups have investigated the adhesion of T cells to supported membranes with anchored MHCp and ICAM1 ligands [8, 9, 11, 15], [64]–[68]. The ligand MHCp binds to the TCR and the ligand ICAM1 to the integrin LFA1 in the T-cell membrane. The TCR–MHCp complex has a length of about 13 nm [2], and the LFA1–ICAM1 complex a length of 40 nm [6]. A situation in which two ligands in the supported membrane bind to different receptors in a cell membrane can be described in our model via the interaction energy [20]

$$\mathcal{H}_{\text{int}}\{l, n, m\} = \sum_i (\delta_{n_i,1} \delta_{m_i,1} V_1(l_i) + \delta_{n_i,2} \delta_{m_i,2} V_2(l_i)). \quad (20)$$

Here, the occupation number $n_i = 1, 2$ or 0 indicates whether a receptor R_1 , a receptor R_2 or no receptor is present in patch i of the cell membrane in the contact zone, while $m_i = 1, 2$ or 0 indicates whether a ligand L_1 , a ligand L_2 or no ligand is present in the apposing patch i of the supported membrane. The interaction of a receptor R_1 with an apposing ligand L_1 is described by the potential $V_1(l_i)$, and the interaction of R_2 with L_2 by the potential $V_2(l_i)$. As in section 4.2, a summation over all possible distributions n and m of receptors and ligands in the partition function leads to an effective double-well potential of the membranes. The effective potential has the same form as in figure 4(b), but the depths of the two wells

$$U_1^{\text{ef}} \approx k_B T [R_1][L_1] K_1 \quad (21)$$

and

$$U_2^{\text{ef}} \approx k_B T [R_2][L_2] K_2 \quad (22)$$

now depend on the concentrations $[R_1]$ and $[R_2]$ of unbound receptors in the cell membrane, on the concentrations $[L_1]$ and $[L_2]$ of unbound ligands in the supported membrane and on the binding constants $K_1 = a^2 e^{U_1/k_B T}$ and $K_2 = a^2 e^{U_2/k_B T}$ for the complexes $R_1 L_1$ and $R_2 L_2$ [19].

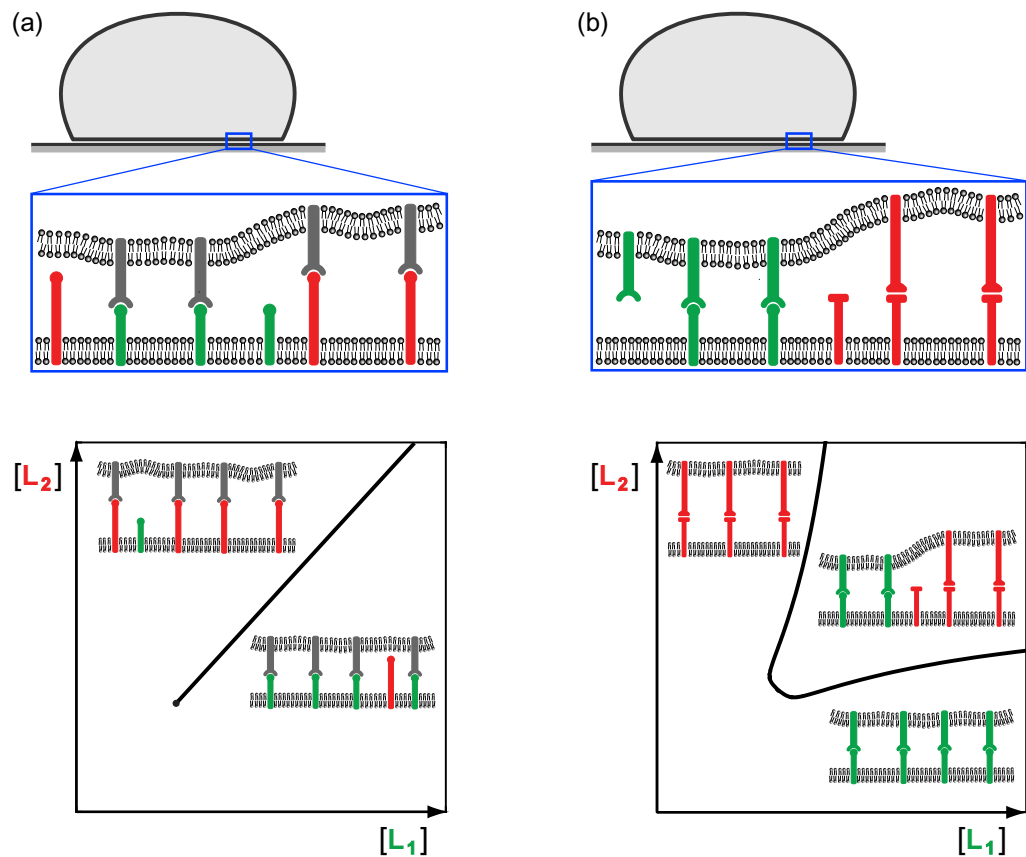


Figure 5. (a) A supported membrane with two types of ligands, L_1 and L_2 , which bind to the same receptor R of an adhering cell (top). The different length of the ligands causes a membrane-mediated repulsion between the receptor–ligand complexes RL_1 and RL_2 . For sufficiently large concentrations $[L_1]$ and $[L_2]$ of the ligands, the repulsion of the complexes RL_1 and RL_2 leads to the formation of domains. However, domain coexistence in the cell adhesion zone only occurs for equal effective binding strengths $K_1[L_1] = K_2[L_2]$ of the ligands. Here, K_1 and K_2 are the binding equilibrium constants of the two ligands at appropriate membrane separations. Domain coexistence thus occurs along the shown line with slope K_1/K_2 in the $[L_1]$ – $[L_2]$ -plane (bottom). The line ends at the critical point for domain formation. For $K_1[L_1] > K_2[L_2]$, the adhesion is dominated by the ligand L_1 throughout the cell adhesion zone, and by the ligand L_2 for $K_1[L_1] < K_2[L_2]$. We have assumed here that the supported membrane is large compared to the adhesion zone, which implies that the concentrations $[L_1]$ and $[L_2]$ of unbound ligands do not change significantly upon adhesion. (b) A supported membrane with two types of ligands, L_1 and L_2 , which bind to different cell receptors R_1 and R_2 . Domain coexistence in the cell adhesion zone now occurs for $K_1[R_1][L_1] = K_2[R_2][L_2]$, which leads to a broad coexistence region in the $[L_1]$ – $[L_2]$ -plane since the concentrations of unbound receptors $[R_1]$ and $[R_2]$ depend on the numbers of bound receptors and, thus, on the adhesion zone fractions occupied by the two domains.

5.2. Phase diagram

As in section 4.3, domain coexistence in the cell contact zone requires equal depths $U_1^{\text{ef}} = U_2^{\text{ef}}$ of the potential wells if the two wells have the same width l_{we} . The effective adhesion potential is then a symmetric double-well potential. We assume here again that the total area of the supported membrane is large compared to the cell contact zone. In this case, the numbers of bound ligands in the contact zone is negligible compared to the numbers of unbound ligands in the total supported membrane, which implies that the concentrations $[L_1]$ and $[L_2]$ of unbound ligands do not change during adhesion. However, the concentrations $[R_1]$ and $[R_2]$ of unbound receptors in general change during cell adhesion, because the contact area is typically a substantial fraction of the overall area of the cell membrane, and because the total numbers N_1 and N_2 of the receptors in the cell membrane are constant. During adhesion, a smaller or larger fraction of the receptors will form bound complexes R_1L_1 or R_2L_2 (see also section 3.4). The concentrations $[R_1L_1]$ and $[R_2L_2]$ of the receptor–ligand complexes in the cell contact area depend on the fractions P_1 and P_2 of the membranes within well 1 and well 2 of the effective adhesion potential. The receptor–ligand complexes R_1L_1 can only form in the membrane fraction P_1 of the contact area within binding range $l_1 \pm l_{\text{we}}/2$ of R_1 and L_1 and the complexes R_2L_2 only in the membrane fraction P_2 within binding range $l_2 \pm l_{\text{we}}/2$ of R_2 and L_2 .

For the symmetric double-well potential with $U_1^{\text{ef}} = U_2^{\text{ef}}$, the membrane fractions P_1 and P_2 within well 1 and well 2 depend primarily on the rescaled potential depth

$$u \equiv U_1^{\text{ef}} \kappa l_{\text{we}}^2 / (k_B T)^2 = U_2^{\text{ef}} \kappa l_{\text{we}}^2 / (k_B T)^2, \quad (23)$$

as in section 3.3. The Monte Carlo data in figure 6(a) illustrate how P_1 and P_2 depend on u . Below the critical potential depth u_c , the membrane fluctuates between the two wells. Because of the symmetry of the potential, P_1 and P_2 attain the same value $P_b(u) \equiv P_1(u) = P_2(u)$ for $u < u_c$. Above the critical potential depth u_c , we have a spontaneous symmetry breaking of the membranes into domains that are predominantly bound in well 1 or well 2, or in other words, predominantly bound by the complexes R_1L_1 or the complexes R_2L_2 . The symmetry breaking for $u > u_c$ is reflected by two branches $P_b^+(u)$ and $P_b^-(u)$ of the membrane fraction $P_b(u)$ within the wells (see figure 6(a)). For the domain predominantly bound in well 1, we have $P_1(u) = P_b^+(u)$ and $P_2(u) = P_b^-(u)$. For the domain predominantly bound in well 2, we have $P_2(u) = P_b^+(u)$ and $P_1(u) = P_b^-(u)$. For $u \gg u_c$, we have $P_b^-(u) \approx 0$ (see figure 6(a)), which implies that domain 1 then contains only the complexes R_1L_1 , and domain 2 only the complexes R_2L_2 .

Since the total numbers N_1 and N_2 of receptors 1 and 2 in the cell membrane are constant, we have

$$N_1 = [R_1]A + K_1[R_1][L_1]A_c (\phi P_b^+(u) + (1 - \phi)P_b^-(u)), \quad (24)$$

$$N_2 = [R_2]A + K_2[R_2][L_2]A_c ((1 - \phi)P_b^+(u) + \phi P_b^-(u)). \quad (25)$$

Here, A is the total area of the cell, A_c is the contact area and ϕ is the fraction of the contact area occupied by domain 1, which is predominantly bound in well 1. The first terms on the right-hand sides, $[R_1]A$ and $[R_2]A$, are the total numbers of unbound receptors. The concentrations $[R_1]$ and $[R_2]$ of unbound receptors within and outside of the contact zone are equal since we neglect the area occupied by bound receptor–ligand complexes within the contact zone

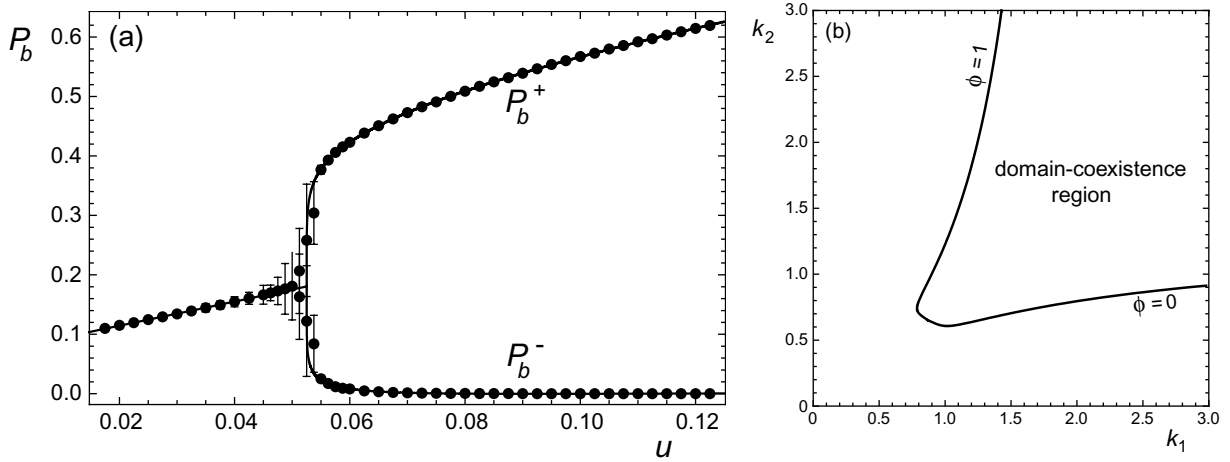


Figure 6. (a) Monte Carlo data for the membrane fraction P_b within the wells of a symmetric double-well potential with rescaled well depth u (see equation (23)). The data are from simulations with the rescaled width $z_{we} = (l_{we}/a)\sqrt{\kappa/k_B T} = 0.5$ and rescaled separation $z_{ba} = (l_{ba}/a)\sqrt{\kappa/k_B T} = 2$ of the two wells. Here, l_{we} and l_{ba} are the width and separation of the wells, a is the linear size of the discrete membrane patches and κ is the effective rigidity of the membranes. Below the critical well depth $u_c \approx 0.053$, the membrane is bound in both wells with the same fraction $P_b(u)$. Above the critical well depth u_c , the membrane is predominantly bound in one of the two wells. The membrane fraction bound in the dominant well is $P_b^+(u)$ (upper branch for $u > u_c$), and the membrane fraction bound in the other well is $P_b^-(u)$ (lower branch for $u > u_c$). We have obtained the data from simulations with a square lattice of up to 200×200 membrane patches and with up to 5×10^7 Monte Carlo steps per lattice site. Details of the Monte Carlo simulations are described in [18, 21]. (b) Exemplary phase diagram for the rescaled receptor numbers $n_1 = 0.07$ and $n_2 = 0.09$ (see equation (26)) obtained from interpolation of the Monte Carlo data in (a) and insertion of the functions $P_b^+(u)$ and $P_b^-(u)$ in equations (33) and (34). Here, k_1 and k_2 are the rescaled concentrations of the two ligands in the supported membrane (see equation (27)). The two-phase coexistence region is bounded by two lines along which the area fraction ϕ of domain 1 in the contact zone is $\phi = 0$ and $\phi = 1$ (see equations (33) and (34)).

(see also equation (11)). The second terms on the right-hand sides of equations (24) and (25) are the numbers of bound receptors. In analogy to equation (7), the number of bound receptors R_1 in the domain predominantly bound in well 1 is $K_1[R_1][L_1]A_c\phi P_b^+(u)$, and the number of bound receptors R_2 in this domain is $K_2[R_2][L_2]A_c\phi P_b^-(u)$. The number of bound receptors R_1 in the domain that is predominantly bound in well 2 is $K_1[R_1][L_1]A_c(1-\phi)P_b^-(u)$, and the number of bound receptors R_2 in this domain is $K_2[R_2][L_2]A_c(1-\phi)P_b^+(u)$. Below the critical potential depth u_c , we have $P_b^+(u) = P_b^-(u) = P_b(u)$. The two equations (24) and (25) therefore are independent of each other for $u < u_c$, but dependent on each other for $u > u_c$.

With the four independent, dimensionless parameters

$$n_1 = \frac{N_1 \kappa l_{\text{we}}^2}{A_c k_B T}, \quad n_2 = \frac{N_2 \kappa l_{\text{we}}^2}{A_c k_B T} \quad (26)$$

and

$$k_1 = K_1 [L_1] \frac{A_c}{A}, \quad k_2 = K_2 [L_2] \frac{A_c}{A}, \quad (27)$$

equations (24) and (25) can be rewritten as

$$n_1 = \frac{u}{k_1} + u (\phi P_b^+(u) + (1 - \phi) P_b^-(u)), \quad (28)$$

$$n_2 = \frac{u}{k_2} + u ((1 - \phi) P_b^+(u) + \phi P_b^-(u)), \quad (29)$$

since we have $u = K_1 [R_1] [L_1] l_{\text{we}}^2 \kappa / k_B T = K_2 [R_2] [L_2] l_{\text{we}}^2 \kappa / k_B T$ (see equations (21)–(23)). From these two equations, one can determine u and ϕ as functions of the independent parameters n_1, n_2, k_1 and k_2 . Domain coexistence in the cell contact zone occurs for $u > u_c$ and $0 < \phi < 1$.

To obtain general relations for the critical point and the boundary lines of the two-phase region in the k_1 – k_2 plane, we first solve equation (28) for k_1 and equation (29) for k_2 , which leads to

$$k_1 = \frac{u}{n_1 - u (\phi P_b^+(u) + (1 - \phi) P_b^-(u))}, \quad (30)$$

$$k_2 = \frac{u}{n_2 - u ((1 - \phi) P_b^+(u) + \phi P_b^-(u))}. \quad (31)$$

At the critical point, we have $P_b^+(u_c) = P_b^-(u_c) = P_b(u_c)$. By inserting these relations into equations (30) and (31), we obtain a general expression for the location $(k_1, k_2)_c$ of the critical point in the k_1 – k_2 plane:

$$(k_1, k_2)_c = \left(\frac{u_c}{n_1 - u_c P_b(u_c)}, \frac{u_c}{n_2 - u_c P_b(u_c)} \right). \quad (32)$$

For the Monte Carlo data of figure 6(a) with $u_c \simeq 0.053$ and $P_b(u_c) \simeq 0.18$, for example, we have $(k_1, k_2)_c \simeq (0.053/(n_1 - 0.0095), 0.053/(n_2 - 0.0095))$. Since k_1 and k_2 have to be positive, domain coexistence can only occur if n_1 and n_2 are both larger than $u_c P_b(u_c)$. The domain-coexistence region in the k_1 – k_2 plane is bounded by two lines with $\phi = 0$ and $\phi = 1$. Inserting $\phi = 0$ in equations (30) and (31) leads to the parametric form

$$(k_1, k_2)_{\phi=0} = \left(\frac{u}{n_1 - u P_b^-(u)}, \frac{u}{n_2 - u P_b^+(u)} \right) \quad \text{for } u > u_c \quad (33)$$

for the $\phi = 0$ line. Similarly, inserting $\phi = 1$ in equations (30) and (31) leads to the parametric form

$$(k_1, k_2)_{\phi=1} = \left(\frac{u}{n_1 - u P_b^+(u)}, \frac{u}{n_2 - u P_b^-(u)} \right) \quad \text{for } u > u_c \quad (34)$$

for the $\phi = 1$ line. The domain-coexistence region in the phase diagram of figure 6(b), for example, follows from inserting the functions $P_b^+(u)$ and $P_b^-(u)$ obtained from interpolation of the Monte Carlo data shown in figure 6(a) into equations (33) and (34).

For $u \gg u_c$, we have $P_b^-(u) \approx 0$. The $\phi = 0$ line then is given by

$$k_2 \Big|_{\phi=0} \approx \frac{k_1 n_1}{n_2 - k_1 n_1 P_b^+(k_1 n_1)}, \quad (35)$$

since we have $u \approx k_1 n_1$ for $P_b^-(u) \approx 0$. Similarly, the $\phi = 1$ line is given by

$$k_1 \Big|_{\phi=1} \approx \frac{k_2 n_2}{n_1 - k_2 n_2 P_b^+(k_2 n_2)} \quad (36)$$

because of $u \approx k_2 n_2$. For $u \gg u_c$, the membranes are only bound via one of the wells. The membrane fraction P_b^+ bound in this well can therefore be approximated by the same expression $P_b^+(u) \approx u/(c_1 + u)$ with $c_1 \simeq 0.071$, as in the case of an effective single-well adhesion potential (see equation (9)).

The $\phi = 0$ line has a vertical asymptote in the k_1 - k_2 plane, since k_2 in equation (35) diverges for

$$n_2 = k_1 n_1 P_b^+(k_1 n_1) \quad (37)$$

because the denominator of the right-hand side of equation (31) vanishes. With $P_b^+(u) \approx u/(c_1 + u)$, we obtain the location

$$k_1 \approx \frac{n_2}{2n_1} \left(1 + \sqrt{1 + 4 \frac{c_1}{n_2}} \right) \quad (38)$$

for this vertical asymptote from equation (37). Similarly, the $\phi = 1$ line has a horizontal asymptote in the k_1 - k_2 plane since the denominator of the right-hand side of equation (36) vanishes for

$$n_1 = k_2 n_2 P_b^+(k_2 n_2). \quad (39)$$

With $P_b^+(u) \approx u/(c_1 + u)$, we obtain the value

$$k_2 \approx \frac{n_1}{2n_2} \left(1 + \sqrt{1 + 4 \frac{c_1}{n_1}} \right) \quad (40)$$

for the horizontal asymptote of the $\phi = 1$ line from equation (39).

6. Discussion and conclusions

In this paper, we have determined phase diagrams for cells adhering to supported membranes with anchored ligands. For supported membranes with short and long ligands L_1 and L_2 that bind to the same cell receptor R , coexistence of domains of L_1R and L_2R complexes in the cell adhesion zone only occurs for equal effective binding strength $K_1[L_1] = K_2[L_2]$ of the complexes where K_1 and K_2 are the binding equilibrium constants at appropriate membrane separations. The domain coexistence thus occurs along a line in the $[L_1]$ - $[L_2]$ plane, which ends at the critical point (see figure 5(a)). We have assumed that the area of the supported membrane is much larger than the adhesion zone, which implies that the concentrations $[L_1]$ and $[L_2]$ of unbound ligands do not change significantly during adhesion since the supported membrane constitutes a large ‘ligand reservoir’. Constant concentrations of unbound

ligands imply constant chemical potentials $\mu_1 \approx k_B T \ln(a^2[L_1])$ and $\mu_2 \approx k_B T \ln(a^2[L_2])$ for the ligands in our model (see equation (32) in [21]). A coexistence line as in the diagram of figure 5(a) is typical for phase diagrams in grand-canonical ensembles with constant chemical potentials.

For supported membranes with two types of ligands L_1 and L_2 that bind to different cell receptors R_1 and R_2 , we obtain a qualitatively different phase diagram with a broad coexistence region (see figure 5(b)). Domain coexistence in the cell adhesion zone occurs for $K_1[R_1][L_1] = K_2[R_2][L_2]$. The broad coexistence region is a consequence of the fact that the concentrations of unbound receptors $[R_1]$ and $[R_2]$ depend on the numbers of bound receptors and, therefore, on the fractions of the cell adhesion zone occupied by the domains of R_1L_1 and R_2L_2 complexes, since the total numbers N_1 and N_2 of receptors in the cell membrane are constant. A broad coexistence region as in the diagram of figure 5(b) is typical for phase diagrams in canonical ensembles with constant particle numbers.

Milstein *et al* [5] have observed domain coexistence for a narrow concentration ratio of short and long ligands that bind to the same cell receptor CD2, in agreement with our phase diagram in figure 5(a). However, there are two differences between our phase diagram in figure 5(a) and the phase diagram of Milstein *et al* in figure 7 of [5]. Firstly, the coexistence line in the phase diagram of Milstein *et al* seems to have a finite width. Such a finite width may result from slight changes of the ligand concentrations upon binding, since several cells adhere to the same supported membrane in the experiments. Secondly, the coexistence line in the diagram of Milstein *et al* ends in a region in which the cells do not adhere, while the coexistence line in the diagram of figure 5(a) ends at a critical point. In this paper, we have neglected repulsive interactions from, e.g., the cell glycocalyx. In our model, such repulsive interactions lead to an unbinding of the membranes at certain well depths U_1^{ef} and U_2^{ef} of the effective adhesion potential shown in figure 4 [20]. We obtain a phase diagram similar to the diagram of Milstein *et al* if the well depths U_1^{ef} and U_2^{ef} at which the membranes unbind are larger than the critical potential depth U_c^{ef} , which determines the location of the critical point in the diagram of figure 5(a).

We find that thermal membrane shape fluctuations on the nanometer scale play a central role during cell adhesion. Fluctuations on these scales have been recently reported for immune cells adhering to coated substrates [69, 70]. In previous works, we have found that the fluctuations lead to a cooperative binding of receptors and ligands (see figure 3) [21] and to a critical point for the segregation of long and short receptor–ligand complexes [19, 20]. Our phase diagrams in figure 5 are therefore qualitatively different from phase diagrams calculated with shape fluctuations neglected [43]. The binding cooperativity of receptors and ligands arises since a receptor–ligand complex locally constrains the membrane shape fluctuations and facilitates the binding of nearby complexes. The binding cooperativity is thus closely related to the fluctuation-induced attractive interactions between bound receptor–ligand complexes [17, 18, 29, 71, 72], which result from a suppression of membrane-shape fluctuations, similar to the fluctuation-induced interactions of rigid membrane inclusions [73]–[76].

We have neglected here the line tension of the domain boundaries, which may suppress the formation of small domains in the cell adhesion zone. In classical nucleation theory, the line tension leads to a threshold size for stable domains. Experimental observations of stable microdomains in the adhesion zones of immune cells [9, 13, 65, 67] indicate that this threshold size is rather small. We will consider the line tension between domains of short and long receptor–ligand complexes in detail in a future paper.

References

- [1] Springer T A 1990 Adhesion receptors of the immune system *Nature* **346** 425–34
- [2] Garcia K C, Degano M, Stanfield R L, Brunmark A, Jackson M R, Peterson P A, Teyton L and Wilson I A 1996 An $\alpha\beta$ T cell receptor structure at 2.5 Å and its orientation in the TCR–MHC complex *Science* **274** 209–19
- [3] van der Merwe P A, McNamee P N, Davies E A, Barclay A N and Davis S J 1995 Topology of the CD2–CD48 cell–adhesion molecule complex: implications for antigen recognition by T cells *Curr. Biol.* **5** 74–84
- [4] Wang J H, Smolyar A, Tan K, Liu J H, Kim M, Sun Z Y, Wagner G and Reinherz E L 1999 Structure of a heterophilic adhesion complex between the human CD2 and CD58 (LFA-3) counterreceptors *Cell* **97** 791–803
- [5] Milstein O *et al* 2008 Nanoscale increases in CD2–CD48-mediated intermembrane spacing decrease adhesion and reorganize the immunological synapse *J. Biol. Chem.* **283** 34414–22
- [6] Dustin M L and Cooper J A 2000 The immunological synapse and the actin cytoskeleton: molecular hardware for T cell signaling *Nat. Immunol.* **1** 23–9
- [7] Monks C R, Freiberg B A, Kupfer H, Sciaky N and Kupfer A 1998 Three-dimensional segregation of supramolecular activation clusters in T cells *Nature* **395** 82–6
- [8] Grakoui A, Bromley S K, Sumen C, Davis M M, Shaw A S, Allen P M and Dustin M L 1999 The immunological synapse: a molecular machine controlling T cell activation *Science* **285** 221–27
- [9] Mossman K D, Campi G, Groves J T and Dustin M L 2005 Altered TCR signaling from geometrically repatterned immunological synapses *Science* **310** 1191–93
- [10] Kaizuka Y, Douglass A D, Varma R, Dustin M L and Vale R D 2007 Mechanisms for segregating T cell receptor and adhesion molecules during immunological synapse formation in Jurkat T cells *Proc. Natl Acad. Sci. USA* **104** 20296–301
- [11] DeMond A L, Mossman K D, Starr T, Dustin M L and Groves J T 2008 T cell receptor microcluster transport through molecular mazes reveals mechanism of translocation *Biophys. J.* **94** 3286–92
- [12] Douglass A D and Vale R D 2005 Single-molecule microscopy reveals plasma membrane microdomains created by protein–protein networks that exclude or trap signaling molecules in T cells *Cell* **121** 937–50
- [13] Campi G, Varma R and Dustin M L 2005 Actin and agonist MHC–peptide complex-dependent T cell receptor microclusters as scaffolds for signaling *J. Exp. Med.* **202** 1031–36
- [14] Choudhuri K, Wiseman D, Brown M H, Gould K and van der Merwe P A 2005 T-cell receptor triggering is critically dependent on the dimensions of its peptide–MHC ligand *Nature* **436** 578–82
- [15] Hailman E, Burack W R, Shaw A S, Dustin M L and Allen P M 2002 Immature CD4⁺CD8⁺ thymocytes form a multifocal immunological synapse with sustained tyrosine phosphorylation *Immunity* **16** 839–48
- [16] Lipowsky R 1996 Adhesion of membranes via anchored stickers *Phys. Rev. Lett.* **77** 1652–5
- [17] Weigl T R and Lipowsky R 2001 Adhesion-induced phase behavior of multicomponent membranes *Phys. Rev. E* **64** 011903
- [18] Weigl T R and Lipowsky R 2006 Membrane adhesion and domain formation *Advances in Planar Lipid Bilayers and Liposomes* ed A Leitmannova Liu (New York: Academic)
- [19] Weigl T R, Asfaw M, Krobath H, Rózycki B and Lipowsky R 2009 Adhesion of membranes via receptor–ligand complexes: domain formation, binding cooperativity, and active processes *Soft Matter* **5** 3213–24
- [20] Asfaw M, Rózycki B, Lipowsky R and Weigl T R 2006 Membrane adhesion via competing receptor/ligand bonds *Europhys. Lett.* **76** 703–9
- [21] Krobath H, Rózycki B, Lipowsky R and Weigl T R 2009 Binding cooperativity of membrane adhesion receptors *Soft Matter* **5** 3354–61
- [22] Lipowsky R 1995 Generic interactions of flexible membranes *Handbook of Biological Physics* vol 1 ed R Lipowsky and E Sackmann (Amsterdam: Elsevier)

- [23] Krobath H, Schütz G J, Lipowsky R and Weigl T R 2007 Lateral diffusion of receptor–ligand bonds in membrane adhesion zones: effect of thermal membrane roughness *Europhys. Lett.* **78** 38003
- [24] Gov N, Zilman A G and Safran S 2003 Cytoskeleton confinement and tension of red blood cell membranes *Phys. Rev. Lett.* **90** 228101
- [25] Fournier J-B, Lacoste E and Raphael D 2004 Fluctuation spectrum of fluid membranes coupled to an elastic meshwork: jump of the effective surface tension at the mesh size *Phys. Rev. Lett.* **92** 018102
- [26] Lin L C-L and Brown F L H 2004 Dynamics of pinned membranes with application to protein diffusion on the surface of red blood cells *Biophys. J.* **86** 764–80
- [27] Auth T, Safran S A and Gov N S 2007 Fluctuations of coupled fluid and solid membranes with application to red blood cells *Phys. Rev. E* **76** 051910
- [28] Alberts B, Johnson A, Lewis J, Raff M, Roberts K and Walter P 2002 *Molecular Biology of the Cell* 4th ed (New York: Garland)
- [29] Weigl T R, Netz R R and Lipowsky R 2000 Unbinding transitions and phase separation of multicomponent membranes *Phys. Rev. E* **62** R45–8
- [30] Weigl T R, Andelman D, Komura S and Lipowsky R 2002 Adhesion of membranes with competing specific and generic interactions *Eur. Phys. J. E* **8** 59–66
- [31] Smith A-S and Seifert U 2005 Effective adhesion strength of specifically bound vesicles *Phys. Rev. E* **71** 061902
- [32] Różycki B, Lipowsky R and Weigl T R 2006 Adhesion of membranes with active stickers *Phys. Rev. Lett.* **96** 048101
- [33] Tsourkas P K, Baumgarth N, Simon S I and Raychaudhuri S 2007 Mechanisms of B-cell synapse formation predicted by Monte Carlo simulation *Biophys. J.* **92** 4196–208
- [34] Tsourkas P K, Longo M L and Raychaudhuri S 2008 Monte Carlo study of single molecule diffusion can elucidate the mechanism of B cell synapse formation *Biophys. J.* **95** 1118–25
- [35] Reister-Gottfried E, Sengupta K, Lorz B, Sackmann E, Seifert U and Smith A S 2008 Dynamics of specific vesicle–substrate adhesion: from local events to global dynamics *Phys. Rev. Lett.* **101** 208103
- [36] Asfaw M and Chen H-Y 2009 Adhesion-induced lateral phase separation of multicomponent membranes: the effect of repellers and confinement *Phys. Rev. E* **79** 041917
- [37] Goetz R, Gompper G and Lipowsky R 1999 Mobility and elasticity of self-assembled membranes *Phys. Rev. Lett.* **82** 221–4
- [38] Bell G I 1978 Models for the specific adhesion of cells to cells *Science* **200** 618–27
- [39] Bell G I, Dembo M and Bongrand P 1984 Cell adhesion. Competition between nonspecific repulsion and specific bonding *Biophys. J.* **45** 1051–64
- [40] Komura S and Andelman D 2000 Adhesion-induced lateral phase separation in membranes *Eur. Phys. J. E* **3** 259–71
- [41] Bruinsma R, Behrisch A and Sackmann E 2000 Adhesive switching of membranes: experiment and theory *Phys. Rev. E* **61** 4253–67
- [42] Chen H-Y 2003 Adhesion-induced phase separation of multiple species of membrane junctions *Phys. Rev. E* **67** 031919
- [43] Coombs D, Dembo M, Wofsy C and Goldstein B 2004 Equilibrium thermodynamics of cell–cell adhesion mediated by multiple ligand–receptor pairs *Biophys. J.* **86** 1408–23
- [44] Shenoy V B and Freund L B 2005 Growth and shape stability of a biological membrane adhesion complex in the diffusion-mediated regime *Proc. Natl Acad. Sci. USA* **102** 3213–18
- [45] Wu J-Y and Chen H-Y 2006 Membrane-adhesion-induced phase separation of two species of junctions *Phys. Rev. E* **73** 011914
- [46] Zhang C-Z and Wang Z-G 2008 Nucleation of membrane adhesions *Phys. Rev. E* **77** 021906
- [47] Xu G-K, Feng X-Q, Zhao H-P and Li B 2009 Theoretical study of the competition between cell–cell and cell–matrix adhesions *Phys. Rev. E* **80** 011921
- [48] Atilgan E and Ovrzyn B 2009 Nucleation and growth of integrin adhesions *Biophys. J.* **96** 3555–72

- [49] Dustin M L, Ferguson L M, Chan P Y, Springer T A and Golan D E 1996 Visualization of CD2 interaction with LFA-3 and determination of the two-dimensional dissociation constant for adhesion receptors in a contact area *J. Cell. Biol.* **132** 465–74
- [50] Zhu D-M, Dustin M L, Cairo C W and Golan D E 2007 Analysis of two-dimensional dissociation constant of laterally mobile cell adhesion molecules *Biophys. J.* **92** 1022–34
- [51] Tolentino T P, Wu J, Zarnitsyna V I, Fang Y, Dustin M L and Zhu C 2008 Measuring diffusion and binding kinetics by contact area FRAP *Biophys. J.* **95** 920–30
- [52] Albersdörfer A, Feder T and Sackmann E 1997 Adhesion-induced domain formation by interplay of long-range repulsion and short-range attraction force: a model membrane study *Biophys. J.* **73** 245–57
- [53] Kloboucek A, Behrisch A, Faix J and Sackmann E 1999 Adhesion-induced receptor segregation and adhesion plaque formation: a model membrane study *Biophys. J.* **77** 2311–28
- [54] Maier C W, Behrisch A, Kloboucek A, Simson D A and Merkel R 2001 Specific biomembrane adhesion—indirect lateral interactions between bound receptor molecules *Eur. Phys. J. E* **6** 273–6
- [55] Smith A-S, Lorz B G, Seifert U and Sackmann E 2006 Antagonist-induced deadhesion of specifically adhered vesicles *Biophys. J.* **90** 1064–80
- [56] Lorz B G, Smith A-S, Gege C and Sackmann E 2007 Adhesion of giant vesicles mediated by weak binding of Sialyl-Lewis(x) to E-selectin in the presence of repelling poly(ethylene glycol) molecules *Langmuir* **23** 12293–300
- [57] Purrucker O, Goennenwein S, Foertig A, Jordan R, Rusp M, Baermann M, Moroder L, Sackmann E and Tanaka M 2007 Polymer-tethered membranes as quantitative models for the study of integrin-mediated cell adhesion *Soft Matter* **3** 333–6
- [58] Smith A-S, Sengupta K, Goennenwein S, Seifert U and Sackmann E 2008 Force-induced growth of adhesion domains is controlled by receptor mobility *Proc. Natl Acad. Sci. USA* **105** 6906–11
- [59] Fenz S F, Merkel R and Sengupta K 2009 Diffusion and intermembrane distance: case study of avidin and E-cadherin mediated adhesion *Langmuir* **25** 1074–85
- [60] Monzel C, Fenz S F, Merkel R and Sengupta K 2009 Probing biomembrane dynamics by dual-wavelength reflection interference contrast microscopy *ChemPhysChem* **10** 2828–38
- [61] Streicher P, Nassoy P, Bärmann M, Dif A, Marchi-Artzner V, Brochard-Wyart F, Spatz J and Bassereau P 2009 Integrin reconstituted in GUVs: a biomimetic system to study initial steps of cell spreading *Biochim. Biophys. Acta* **1788** 2291–300
- [62] Smith A-S, Fenz S F and Sengupta K 2010 Inferring spatial organization of bonds within adhesion clusters by exploiting fluctuations of soft interfaces *Europhys. Lett.* **89** 28003
- [63] Lipowsky R 1994 Discontinuous unbinding transitions of flexible membranes *J. Physique II* **4** 1755–62
- [64] Krogsgaard M, Li Q-J, Sumen C, Huppa J B, Huse M and Davis M M 2005 Agonist/endogenous peptide–MHC heterodimers drive T cell activation and sensitivity *Nature* **434** 238–43
- [65] Yokosuka T, Sakata-Sogawa K, Kobayashi W, Hiroshima M, Hashimoto-Tane A, Tokunaga M, Dustin M L and Saito T 2005 Newly generated T cell receptor microclusters initiate and sustain T cell activation by recruitment of Zap70 and SLP-76 *Nat. Immunol.* **6** 1253–62
- [66] Varma R, Campi G, Yokosuka T, Saito T and Dustin M L 2006 T cell receptor-proximal signals are sustained in peripheral microclusters and terminated in the central supramolecular activation cluster *Immunity* **25** 117–27
- [67] Yokosuka T, Kobayashi W, Sakata-Sogawa K, Takamatsu M, Hashimoto-Tane A, Dustin M L, Tokunaga M and Saito T 2008 Spatiotemporal regulation of T cell costimulation by TCR–CD28 microclusters and protein kinase C theta translocation *Immunity* **29** 589–601
- [68] Huppa J B, Axmann M, Mörtelmaier M A, Lillemeier B F, Newell E W, Brameshuber M, Klein L O, Schütz G J and Davis M M 2010 TCR–peptide–MHC interactions *in situ* show accelerated kinetics and increased affinity *Nature* **463** 963–7
- [69] Pierres A, Benoliel A-M, Touchard D and Bongrand P 2008 How cells tiptoe on adhesive surfaces before sticking *Biophys. J.* **94** 4114–22

- [70] Pierres A, Monnet-Corti V, Benoliel A-M and Bongrand P 2009 Do membrane undulations help cells probe the world? *Trends Cell Biol.* **19** 428–33
- [71] Bruinsma R, Goulian M and Pincus P 1994 Self-assembly of membrane junctions *Biophys J.* **67** 746–50
- [72] Farago O 2010 Fluctuation-induced attraction between adhesion sites of supported membranes *Phys. Rev. E* **81** 050902
- [73] Goulian M, Bruinsma R and Pincus P 1993 Long-range forces in heterogeneous fluid membranes *Europhys. Lett.* **22** 145–50
- [74] Netz R R and Pincus P 1995 Inhomogeneous fluid membranes: segregation, ordering, and effective rigidity *Phys. Rev. E* **52** 4114–28
- [75] Golestanian R, Goulian M and Kardar M 1996 Fluctuation-induced interactions between rods on a membrane *Phys. Rev. E* **54** 6725–34
- [76] Weikl T R 2001 Fluctuation-induced aggregation of rigid membrane inclusions *Europhys. Lett.* **54** 547–53